11. W. J. Rainbird, "Turbulent boundary layer growth and separation on a yawed cone," AIAA J., 6, No. 12 (1968); RTK, 6, No. 12 (1968).
12. W. B. Sturek and L. B. Schiff, Numerical simulation of steady supersonic flow over spinning bodies of revolution, AIAA J., Vol. 20, No. 12 (1982).
13. D. S. Dolling and W. K. Gray, Experimental study of supersonic turbulent flow on a blunted axisymmetric body, AIAA J., 24, No. 5 (1986).
14. Yu. D. Shevelev, Three-Dimensional Problems of Laminar Boundary Layer Theory [in Russian], Nauka, Moscow (1977).
15. N. D. Vvedenskaya, "Computation of the boundary layer generated in flow over a cone at angle of attack," Zh. VMMF, 6, No. 2 (1966).
16. L. M. Vetlutskaya and V. N. Vetlutskii, "Computation of the three-dimensional compressible laminar boundary layer on a sharp body," ChMMSS, 17, No. 5 (1986).
17. K. C. Wang, "Determination of the zones of influence and dependence for the three-dimensional boundary layer equations," J. Fluid Mech., 48, No. 2 (1971).
18. V. N. Vetlutsky, "Laminar boundary layer on a flat plate with a rotating cylinder," Comp. Fluids, 9, No. 4 (1981).
19. C. H. Reinsch, Smoothing by Spline Functions, Numerische Mathematik (1967), Bd 10.
20. E. Krause, Comment on "Solution of a three-dimensional boundary layer flow with separation," AIAA J., 7, No. 3 (1969).
21. D. Schwamborn, Laminare Grenzschichten in der Nähe der Anlegelinie an Flügeln und flügelähnlichen Körpern mit Anstellung, BRD (1981), (Forschungsbericht, DFVLR, N 81-31).
22. M. K. Aukin and R. K. Tagirov, "Method of computing supersonic flow over a vehicle in the presence of air fences, wings, and fins," ChMMSS, 11, No. 6 (1980).
23. G. Schlichting, Boundary Layer Theory [Russian translation], Nauka, Moscow (1974).

TURBULENT INCOMPRESSIBLE FLUID FLOW IN A CHANNEL WITH UNILATERAL MASS TRANSFER

Sh. A. Ershin, U. K. Zhapbasbaev, T. B. Kozhakhmetov, and A. V. Smol'yaninov

UDC 532.542

The great practical value of channel flows with mass transfer through a porous wall evokes extensive interest [1-3]. If laminar flow analysis can rely on the solution of the exact equations of viscous fluid motion, then the turbulent motions most important in practical respects, are unfortunately not yet subject to a reliable theoretical analysis. Well-founded expectations are bestowed on modern turbulence models whose perfection may result in the possibility of a theoretical computational prediction of many complex turbulent flow modes. However, without a sufficient base of experimental data it is difficult to compute successful forward progress except success should be expected for an obligatory combination of empirical and analytical approaches to the problem. Such empirical material for flows in channels with smooth impermeable walls has been obtained in [4-7] and, for example, with rough walls in [8]. As regards flows in channels with mass transfer through the wall, then insofar as we know analogous investigations are still nonexistent. The present paper is a part of a general investigation of turbulent flow in a plane channel with mass transfer through porous walls.

1. The tests were performed on an apparatus that is a flat channel of width $2B = 0.45$ m and height $2H = 0.034$ m operating in the pressure mode. The fan had a soft connection with an air duct of about 20 m extent, from which air is delivered again through a soft connection to a receiving diffuser at the input of the stabilized channel section 140H in length. Therefore, the possibility is eliminated of transmission of mechanical vibrations from the fan and metal air duct to the apparatus. The metal diffusor is executed according to Vitoshinskii and is connected to the experimental apparatus through a system of networks and gratings. The stabilized channel section is fabricated from 0.03 m wood chip shavings

Alma-Ata. Translated from Zhurnal Prikladnoi Mekhaniki i Tekhnicheskoi Fiziki, No. 1, pp. 62-68, January-February, 1991. Original article submitted March 7, 1989; revision submitted September 29, 1989.

0021-8944/91/3201-0057$12.50

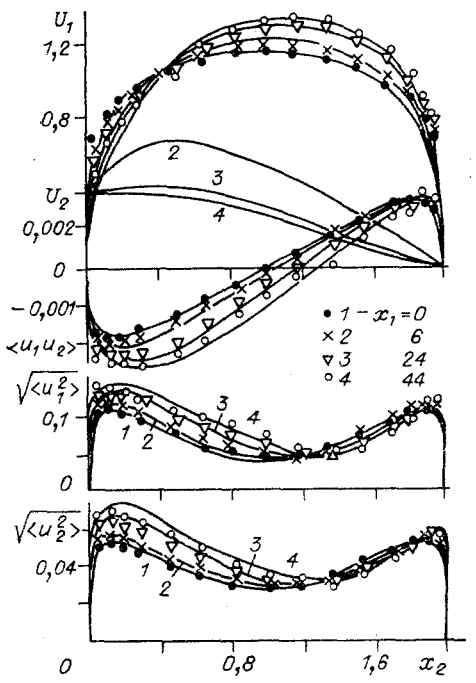

Fig. 1

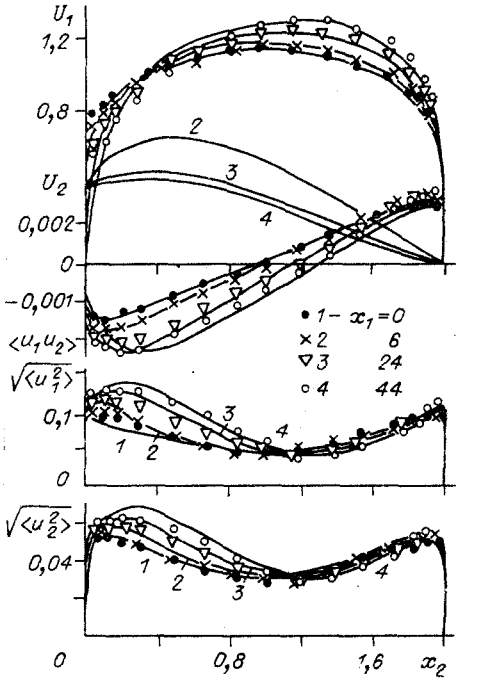

Fig. 2

with polished surfaces, had two junctions, one with the delivery diffusor and the other with the working section. This latter was a natural continuation of the wood part of the channel but one wall was from thick organic glass while the opposite was a porous metal-ceramic plate with porosity factor $\varepsilon_0 = 0.35$ and mean dimension $2 \cdot 10^{-5}$ m for the height of the roughness element. A duct, separated into seven isolated sections along the length of the working section, was fastened hermetically to the outer side of the porous wall of the channel. Injectable air was delivered to each section independently through a rotameter. There were special orifices for the insertion of a measuring thermoanemometer probe on the opposite impermeable wall along the center line of the channel working section. The surface turned within the channel of the sealed plugs was carefully adjusted flush with the channel wall. The measuring probe was a paired single-thread constant resistance sensor that was displaced across the channel by using a microplotter with $5 \cdot 10^{-6}$ m accuracy. One pair of jaws with a filament permitted execution of measurements near the permeable wall, the other at the opposite impermeable wall. The state of the filament, the parallelism of its surface to the channel walls and the distance to the wall as it approached this latter was checked by a V-690 cathetometer to $5 \cdot 10^{-6}$ m accuracy. Cruciform sensors (tungsten filaments of $6 \cdot 10^{-6}$ m diameter and $1.6 \cdot 10^{-3}$ m length) were used to measure the transverse velocity components and the time correlations. The jaws of the single-filament sensors were directed at a 30-35° angle to the channel walls and permitted approaching it to a $4 \cdot 10^{-5}$ m distance, while the cruciform sensor could be brought to $1 \cdot 10^{-3}$ m. Drain holes were along the whole channel for static pressure measurements.

Verification of all the fundamental flow characteristics in the channel with impermeable walls without connecting the working section preceded the tests with mass transfer. They were compared with known tests [4-7]. Analogous measurements were performed with the working section attached without injection. In order to clarify the possible influence of mass transfer on the velocity profile being stabilized prior to entrance into the working section (i.e., upstream), measurements of all the characteristics were performed anew upon entrance into the porous part of the channel under maximal injection. The results of all these test measurements yielded good mutual agreement.

It is known that stabilization of the fluctuation characteristics sets in considerably later than the average. Consequently, besides the measurements across the channel $x_2 = X_2/H$, analogous measurements were performed also along the channel width in the direction $x_3 = X_3/B$. The results showed that flow homogeneity is conserved in all the parameters over more than 80% of the channel width. The data obtained at the entrance to the working section, agree in the absence of mass transfer with the results of measurements at its output to 2-3% accuracy.

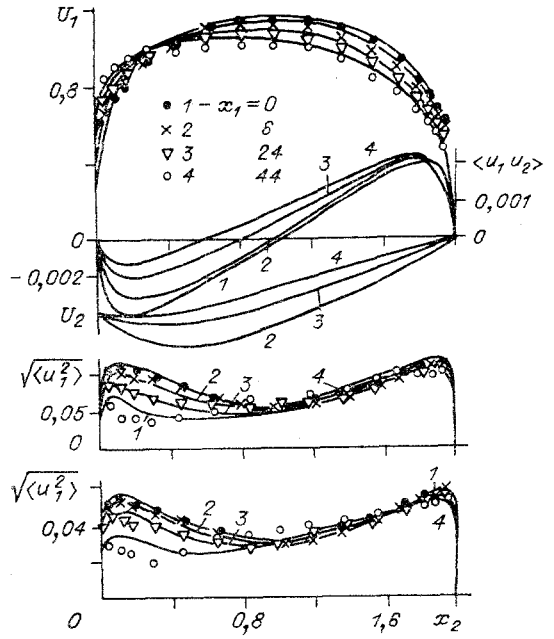

Fig. 3

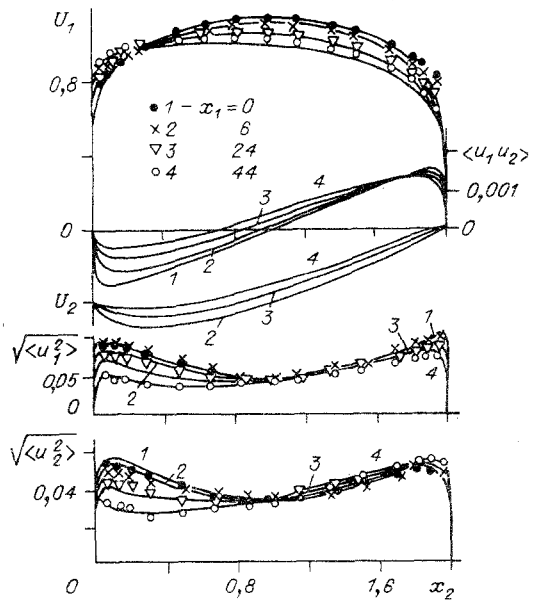

Fig. 4

The possibilities of the apparatus were constrained by the value of the Reynolds number ($Re = U_0H/\nu$) to 47,000 (U_0 is the initial mean mass flow rate of the flow). The main part of the experiments was performed for Re = 4300 and 43,000 and the mass transfer intensity m = ±2, ±4, ±8.8, and ±17.6%, defined as the ratio between the flow rate of the gas injected through the porous wall and the air flow rate of the main flow: $m = Q/Q_0$. Here $Q = v_W LB$; $Q_0 = 4HBU_0$; L is the length of the working section, and v_W is the mass transfer rate. In conformity with these values $Re_W = v_W H/\nu$ equal:

for Re = 4300 $Re_w = \pm 4.36;\ \pm 8.72;\ \pm 21.8;\ \pm 43.6,$

for Re = 43000 $Re_w = \pm 43.6;\ \pm 87.2;\ \pm 218;\ \pm 436.$

The distinguishing feature of channel flow with mass transfer through one wall is the unstabilizability of the motion. The downstream flow rate changes continuously, while the profiles of the longitudinal velocity components are deformed, and the more slowly, the more intensive the mass transfer.

Certain measurement data on injection in transverse sections of the channel working section are presented in Figs. 1 and 2 for m = 17.6% and Re = 4300 and 43,000, respectively. Test profiles of the longitudinal velocity component $U_1 = \bar{U}_1/U_0$ are shown by points at the top and the turbulent flow $\langle u_1 u_2 \rangle = \overline{\langle u_1 u_2 \rangle}/U_0^2$ below, and the rms components of the longitudinal $\sqrt{\langle u_1^2 \rangle} = \sqrt{\langle u_1^2 \rangle}/U_0$ and transverse $\sqrt{\langle u_2^2 \rangle} = \sqrt{\langle u_2^2 \rangle}/U_0$ fluctuating motion velocities, still lower.

Analogous order is conserved for Figs. 3 and 4, where certain test data on suction are constructed for m = –17.6% and Re = 4300 and 43,000. The construction of the figures is unified. The reading is made everywhere from the porous ($x_2 = 0$) to the impermeable wall ($x_2 = 2$) in the figures where results of measurements across the channel in the direction x_2 are represented.

Continuous deformation of the velocity profile U_1 in the channel working section indicates the presence of not only tangential but also normal components of the shear stress. In the injection case, the U_1 profile is forced back from the porous wall and is filled up at the solid wall. The maximum stands off from the axis towards the continuous wall. Gas injection causes growth of the turbulent characteristics near the permeable surface. The magnitude of the turbulent friction $\langle u_1 u_2 \rangle$ and the rms components grow downstream. The zeroth value of $\sqrt{\langle u_1^2 \rangle}$, $\sqrt{\langle u_2^2 \rangle}$ and the minima of $\sqrt{\langle u_1^2 \rangle}$, $\sqrt{\langle u_2^2 \rangle}$ are shifted from the channel axis (see Figs. 1 and 2), where their locations do not agree with the maximum of U_1. They are arranged closer to the continuous wall. Near the continuous wall the quantities

$\langle u_1u_2\rangle$, $\sqrt{\langle u_1^2\rangle}$, $\sqrt{\langle u_2^2\rangle}$ differ insignificantly in different parts of the working section. Deformation of the profiles U_1, $\langle u_1u_2\rangle$, $\sqrt{\langle u_1^2\rangle}$, $\sqrt{\langle u_2^2\rangle}$ is continued along the whole length of the working section, however, as x_1 grows their intensity is lowered. In connection with the filling U_1, the resistance on the continuous wall grows and it will compensate for the rise in $\langle u_1u_2\rangle$ near the permeable surface.

For the values Re = 43,000 and m = 17.6% the nature of the behavior of the experimental data for U_1, $\langle u_1u_2\rangle$, $\sqrt{\langle u_1^2\rangle}$, $\sqrt{\langle u_2^2\rangle}$ is the same for Re = 4300 (see Fig. 2) but the U_1 profiles are more filled in.

As is seen from Figs. 3 and 4, the influence of suction on the flow structure is opposite as compared with injection. Experimental profiles (points) of U_1 gradually becomes shallower downstream. It is known that suction of gas from the boundary layer diminishes the friction resistance on the permeable surface. Consequently, the U_1 profiles are filled up at the porous wall and forced back from the continuous wall. In this connection, the maximum of U_1 is shifted from the axis towards the permeable surface. Test distributions of $\sqrt{\langle u_1^2\rangle}$, $\sqrt{\langle u_2^2\rangle}$ diminish downstream; this is especially noticeable near the porous wall (see Figs. 3 and 4). As experimental data show, suction of the stream results in laminarization of the flow.

2. A computational-theoretical investigation was performed by using a five-parameter model of the turbulent stresses. Let us examine turbulent incompressible fluid motion in a plane channel. We direct the Ox_1 axis along the lower eall and the Ox_2 axis along its height. The fluid motion is described by a system of equations in a narrow channel approximation

$$U_1\frac{\partial U_1}{\partial x_1}+U_2\frac{\partial U_2}{\partial x_2}=-\frac{dP}{dx_1}+\frac{1}{\mathrm{Re}}\frac{\partial^2U_1}{\partial x_2^2}-\frac{\partial\langle u_1^2\rangle}{\partial x_1}-\frac{\partial\langle u_1u_2\rangle}{\partial x_2}; \tag{2.1}$$

$$\partial U_1/\partial x_1+\partial U_2/\partial x_2=0. \tag{2.2}$$

The pressure gradient is found from the integral condition of mass flow rate conservation

$$\int_0^2 U_1\,dx_2=2+V_wx_1 \tag{2.3}$$

($V_W = v_W/U_0$ is the mass transfer parameter).

The system (2.1)-(2.3) is closed by using the model of turbulent stresses [9]. Applied for low Reynolds numbers it has the form

$$U_1\frac{\partial\langle u_iu_j\rangle}{\partial x_1}+U_2\frac{\partial\langle u_iu_j\rangle}{\partial x_2}=\frac{\partial}{\partial x_2}\left(\frac{1}{\mathrm{Re}}\frac{\partial\langle u_iu_j\rangle}{\partial x_2}-J_{ijk}\right)+P_{ij}+\Phi_{ij}-\varepsilon_{ij}, \tag{2.4}$$

where P_{ij} is the generation of turbulent stresses by mean shear, Φ_{ij} is the correlation of pressure fluctuations with deformation rates, J_{ijk} is the molar flow, and ε_{ij} is viscous dissipation. The pressure-deformation correlation term Φ_{ij} is approximated by the formula

$$\begin{aligned}\Phi_{ij}=&-c_1\frac{\varepsilon}{k}\left(\langle u_iu_j\rangle-\frac{2}{3}\delta_{ij}k\right)-\alpha\left(P_{ij}-\frac{2}{3}\delta_{ij}P\right)-\\&-\beta\left(D_{ij}-\frac{2}{3}\delta_{ij}P\right)-\gamma k\left(\frac{\partial U_i}{\partial x_j}+\frac{\partial U_j}{\partial x_i}\right)+\Phi_{ijw}.\end{aligned} \tag{2.5}$$

The following notation is taken here

$$P_{ij}=-\left(\langle u_iu_k\rangle\frac{\partial U_j}{\partial x_k}+\langle u_ju_k\rangle\frac{\partial U_i}{\partial x_k}\right),$$

$$D_{ij} = -\left(\langle u_i u_k\rangle \frac{\partial U_k}{\partial x_j} + \langle u_j u_k\rangle \frac{\partial U_k}{\partial x_i}\right),$$
$$\Phi_{ijw} = \left[c_3\left(P_{ij} - \frac{2}{3}\delta_{ij}P\right) + c_4 k\left(\frac{\partial U_i}{\partial x_j} + \frac{\partial U_j}{\partial x_i}\right)\right] f_w,\ P = P_{kk}/2,\ k = \langle u_i^2\rangle/2 \qquad (2.6)$$

(Φ_{ijw} is the near wall correction to Φ_{ij}, and P is the generation of the kinetic energy of turbulence k).

The diffusion flow is determined by the expression

$$J_{ijk} = -c_s \frac{k}{\varepsilon}\left(\langle u_i u_e\rangle \frac{\partial\langle u_j u_k\rangle}{\partial x_e} + \langle u_j u_e\rangle \frac{\partial\langle u_k u_i\rangle}{\partial x_e} + \langle u_k u_e\rangle \frac{\partial\langle u_i u_j\rangle}{\partial x_e}\right). \qquad (2.7)$$

The equation of dissipation transport of the kinetic energy of turbulence ε is written in the Chien form [10]

$$U_1 \frac{\partial\varepsilon}{\partial x_1} + U_2 \frac{\partial\varepsilon}{\partial x_2} = \frac{\partial}{\partial x_2}\left[\left(\frac{1}{\mathrm{Re}} + c_\sigma \frac{k\langle u_2^2\rangle}{\varepsilon}\right)\frac{\partial\varepsilon}{\partial x_2}\right] + c_{1\varepsilon}\frac{\varepsilon}{k}P - c_{2\varepsilon}f_\vartheta \frac{\varepsilon^2}{k} - \frac{2g_\vartheta\varepsilon}{\mathrm{Re}\,x_2^2} \qquad (2.8)$$

(x_2 is the distance measured from the wall). In conformity with (2,8) the viscous dissipation term ε_{ij} is determined by the formula

$$\varepsilon_{ij} = \frac{2}{3}\delta_{ij}\varepsilon + \frac{2}{\mathrm{Re}}\frac{\delta_{i1}\delta_{jm}}{x_2^2}\langle u_1 u_m\rangle. \qquad (2.9)$$

The equation for the kinetic energy of turbulence, obtained from (2.4) by convolution in the subscripts i and j

$$U_1 \frac{\partial k}{\partial x_1} + U_2 \frac{\partial k}{\partial x_2} = -\langle u_i u_k\rangle \frac{\partial U_i}{\partial x_k} + \frac{\partial}{\partial x_2}\left(\frac{1}{\mathrm{Re}}\frac{\partial k}{\partial x_2} - \frac{J_{ijk}}{2}\right) - \varepsilon - \frac{2k}{\mathrm{Re}\,x_2^2}$$

is used in computations in place of the third turbulent stress component $\langle u_3^2\rangle$.

Constants and near-wall functions $c_1 = 1.5$, $c_2 = 0.4$, $c_3 = 0.45$, $c_4 = 0.08$, $c_S = 0.11$, $c_{1\varepsilon} = 1.35$, $c_{2\varepsilon} = 1.8$, $c_\sigma = 0.15$, $g_e = \exp(-0.5x_2 V_* \mathrm{Re})$, $f_e = 1 - \frac{0.4}{1.8}\exp\left(-\frac{k^2\,\mathrm{Re}}{6\varepsilon}\right)$ ($V_* = v_*/U_0$ is the dynamic velocity in the initial section of the working section) enter into the system (2.4)-(2.9). The constants α, β take on the same values as in [9], while the value of γ is corrected. A better agreement with test is given by $\gamma = (30c_2 - 4.3)/55$.

The near-wall function f_w is determined according to the Cebeci hypotheses [11] and is expressed by the formula

$$f_w = \exp(-2x_2\,\mathrm{Re}\,V_*/A),$$

where $A = 26\left\{-\frac{P_*}{V_{w*}}\exp(11.8V_{w*} - 1) + \exp(11.8V_{w*})\right\}^{-1/2}$; $P_* = -\frac{dP}{dx_1}\frac{1}{\mathrm{Re}\,V_*^3}$; $V_{w*} = V_w/V_*$. For an impermeable wall ($V_{w*} = 0$), there follows $A = 26(1 - 11.8P_*)^{-1/2}$ from the relationship for A.

The system of motion equations (2.1)-(2.3) is solved in combination with the transport equations $\langle u_1^2\rangle$, $\langle u_2^2\rangle$, k, $\langle u_1 u_2\rangle$, ε under the boundary conditions

$$x_1 \geqslant 0, x_2 = 0:\ U_1 = 0, U_2 = V_w, \langle u_1^2\rangle = \langle u_2^2\rangle = \langle u_1 u_2\rangle = k = \varepsilon = 0,$$
$$x_1 \geqslant 0, x_2 = 2:\ U_1 = 0, \langle u_1^2\rangle = \langle u_2^2\rangle = \langle u_1 u_2\rangle = k = \varepsilon = 0.$$

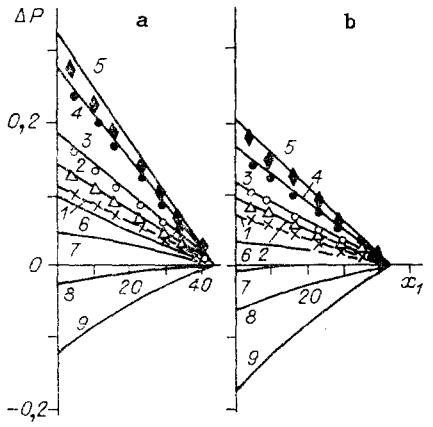

Fig. 5

The boundary conditions at the entrance to the domain with mass transfer are found from the solution of the system of stabilized flow equations in a channel with an impermeable wall.

The system (2.1)-(2.4), (2.8), (2.10) is solved by a numerical method on a nonuniform rectangular mesh constructed according to recommendations in [10]. The minimal mesh spacing in the transverse coordinates is selected with a computation that up to 10 mesh nodes are within the laminar sublayer ($x_2^* \leq 5$). The approximation of the equations was by a two-layer implicit scheme [12]. The pressure gradient was determined by the splitting method [13] from the flow rate conservation condition (2.3).

3. The main mode parameters of the problem are Re and V_w. Computations were performed for fixed Re and V_w in the range $4 \cdot 10^3 \leq \mathrm{Re} \leq 5 \cdot 10^4$ and $-0.01 \leq V_w \leq 0.01$. In conformity with the selection of the coordinate system, negative values of V_w refer to suction and positive values to injection. Comparison of the computation with experiment was along the whole length of the working section (L/H = 44).

A simpler three-parameter turbulance model [9, 14] was drawn upon to generalize the test data. In this case a system of transport equations for $\langle u_1 u_2 \rangle$, k, and ε was solved in combination with (2.1)-(2.3). However, complete agreement of the computation with experiment was not achieved successfully despite the variation in the values of the constants. This is apparently explained by the simplification of the relation between the turbulent flow characteristics and the three-parameter turbulence model.

As is shown above, the model of turbulent stresses under consideration differs from the original modification [9] by the form of the source terms ε_{ij} of turbulence energy dissipation. It must be noted that the initial modification of the model was also relied upon in the computations. Instability of the finite-difference algorithm held during the numerical experiments while the computation of the system (2.1)-(2.4), (2.8), (2.10) was always stable.

The simplicity of the Chien model and its applicability in channel flows were noted in many surveys [15]. Nevertheless, test computations were performed of the system (2.1)-(2.4), (2.8), (2.10), which displayed satisfactory agreement of the computation with known experimental and computed data [5-7, 16].

Computed curves obtained for the same parameters at the test points are presented in Figs. 1-4. Besides the data on U_1, $\langle u_1 u_2 \rangle$, $\sqrt{\langle u_1^2 \rangle}$, $\sqrt{\langle u_2^2 \rangle}$ computation profiles of the transverse velocity component U_2, displaying transverse convection in the flow field are constructed in addition. Attempts to measure U_2 were not successful because of the smallness of their values although the dimensions of the cruciform sensor permitted penetration into the viscous sublayer.

As is seen from Figs. 1-4, the computed curves U_1, $\langle u_1 u_2 \rangle$, $\sqrt{\langle u_1^2 \rangle}$, $\sqrt{\langle u_2^2 \rangle}$ are found in satisfactory agreement with test data in the core of the flow and only near the wall are there certain discrepancies. This can be associated with the disadvantage of the model in the near-wall domain. Nevertheless, the computed data describe the characteristic flow regularities sufficiently well: deformation of the profiles of U_1, U_2, $\langle u_1 u_2 \rangle$, $\sqrt{\langle u_1^2 \rangle}$, $\sqrt{\langle u_2^2 \rangle}$

downstream, shift of the maximum U_1 and the minima of $\sqrt{\langle u_1^2 \rangle}$, $\sqrt{\langle u_2^2 \rangle}$ from the channel axis, non-coincidence of the zero of turbulent friction and the maximum of the longitudinal velocity component U_1, flow turbulization during injection, and conversely, its laminarization during suction.

The change in static pressure in the working part of the channel is given in Fig. 5 for m = 0, 2, 4, 8, 17.6, −2, −4, −8.8, −17.6% (curves 1-9) as well as for Re = 4300 (a) and 43,000 (b). The computed data (lines) show the pressure drop during injection and its restoration in the case of suction along the channel length through the porous wall. Unfortunately, the static pressure was measured in the test for the injection case and as is seen from Fig. 5, the test data agree satisfactorily with the computation.

Therefore, the results of investigations show that the turbulent stress model describes experimental data with acceptable accuracy and it can be used to compute flows with suction and injection.

LITERATURE CITED

1. V. M. Eroshenko and L. M. Zaichik, Hydrodynamics and Heat and Mass Transfer on Permeable Surfaces [in Russian], Nauka, Moscow (1984).
2. S. V. Kalinina, P. P. Lugovskoi, and B. P. Mironov, "Hydrodynamics of the flow in a permeable channel with bilateral injection," Zh. Prikl. Mekh. Tekh. Fiz., No. 6 (1981).
3. V. I. Alimpiev, S. V. Kalinina, and P. P. Lugovskoi, "Investigation of flow hydrodynamics of a single-phase medium in narrow gaps with injection," in: Turbulent Boundary Layer under Complex Boundary Conditions [in Russian], IT Sib. Otd. Akad. Nauk SSSR, Novosibirsk (1977).
4. J. Conte-Bello, Turbulent Flow in a Channel with Parallel Walls [Russian translation], Mir, Moscow (1968).
5. Hussein and Reynolds, "Experimental investigation of completely developed turbulent flow in a channel," TOIR, No. 4 (1975).
6. H. Eckelman, "Structure of the viscous sublayer and the adjacent wall region in a turbulent channel flow," J. Fluid Mech., 65, Pt. 3 (1974).
7. J. Laufer, "Structure of turbulence in fully-developed pipe flow," NACA Rep. No. 1174, New York (1954).
8. K. Hanjalic and B. E. Launder, "Fully developed asymmetric flow in a plane channel," J. Fluid Mech., 52, No. 4 (1972).
9. K. Hanjalic and B. E. Launder, "Contribution towards a Reynolds-stress closure for low Reynolds-number turbulence," J. Fluid Mech., 74, Part 4 (1976).
10. K. Y. Chien, "Predictions of channel and boundary layer flows with a low-Reynolds-number two-equation model of turbulence," AIAA J., 20, No. 1 (1982).
11. T. Cebeci, "Behavior of turbulent flow near a porous wall with pressure gradient," AIAA J., 12, No. 8 (1970).
12. V. M. Paskonov, V. I. Polezhaev, and L. A. Chudov, Numerical Modeling of Heat and Mass Transfer Processes [in Russian], Nauka, Moscow (1984).
13. L. M. Simuni, "Motion of a viscous incompressible fluid in a plane tube," Zh. Vychisl. Mat. Mat. Fiz., 5, No. 6 (1965).
14. V. G. Lushchik, A. A. Pavel'ev, and A. V. Yakubenko, "Three-parameter model of shear turbulence," Izv. Akad. Nauk SSSR, Mekh. Zhidk. Gaza, No. 5 (1978).
15. V. K. Peitel, W. Roddy, and H. Scheuerer, "Turbulence models for flows in a near-wall domain with low Reynolds number. Survey," Aerospace Engineering [Russian translation], No. 2 (1986).
16. U. K. Zhapbasbaev, T. B. Kozhakhmetov, and A. V. Smol'yaninov, "Flow analysis in channels on the basis of a turbulent stress model applicable for low Reynolds numbers," Izv. Akad. Nauk KazSSR, Ser. Fiz.-Mat., No. 3 (1989).